THE JOURNAL OF PHYSICAL CHEMISTRY C

Article

pubs.acs.org/JPCC

What Is the Optoelectronic Effect of the Capsule on the Guest Molecule in Aqueous Host/Guest Complexes? A Combined Computational and Spectroscopic Perspective

Srijana Bhandari,[†] Zilong Zheng,[†] Buddhadev Maiti,[†] Chi-Hung Chuang,[‡] Mintu Porel,[∥] Zhi-Qiang You,[§,⊥] Vaidhyanathan Ramamurthy,*[,∥] Clemens Burda,*[,‡] John M. Herbert,*[,§] and Barry D. Dunietz*[,†]

[†]Department of Chemistry and Biochemistry, Kent State University, Kent, Ohio 44242, United States

[‡]Department of Chemistry and Biochemistry, Case Western Reserve University, Cleveland, Ohio 44106, United States

[§]Department of Chemistry and Biochemistry, The Ohio State University, Columbus, Ohio 43210, United States

[∥]Department of Chemistry, University of Miami, Miami, Florida 33124, United States

Supporting Information

ABSTRACT: Encapsulation of dye molecules is used as a means to achieve charge separation across different dielectric environments. We analyze the absorption and emission spectra of several coumarin molecules that are encapsulated within an octa-acid dimer forming a molecular capsule. The water-solvated capsule effect on the coumarin's electronic structure and absorption spectra can be understood as due to an effective dielectric constant where the capsule partially shields electrostatically the dielectric solvent environment. Blue-shifted emission spectra are explained as resulting from a partial intermolecular charge transfer where the capsule is the acceptor, and which reduces the coumarin relaxation in the excited state.

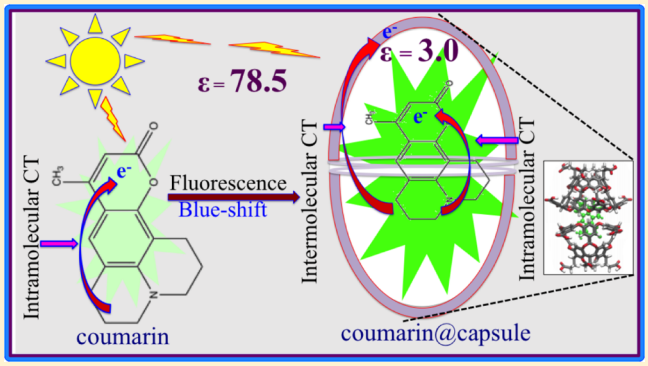

INTRODUCTION

Creating and maintaining an effective and robust interface between donor and acceptor moieties of a charge transfer (CT) process is a key challenge to advancing optoelectronics applications and research.[1] Donor and acceptor moieties have been coupled through molecular bridge chemical synthesis,[2−7] and more recently interfaces consisting of molecular cages and supramolecular assemblies were used to facilitate CT between nonpolar donors and water-soluble acceptors.[8−10] The molecular encapsulation also offers a means to tune optoelectronic properties through control of the interaction between the donor and acceptor moieties. For example, encapsulation can assist charge separation in photovoltaic systems by limiting competing charge recombination processes.[11]

One of our groups has recently encapsulated coumarin (C) dyes in a cavity formed by a dimer of octa-acids (OA_2).[12] In these C−OA_2 complexes, the nonpolar coumarin is protected, while being effectively solvated in water through the capsule hydrophilic outer layer. The hydrophobic protective inner shell of OA_2 consists of aromatic rings creating a relatively inert chemical environment, while the hydrophilic outer shell consists of 16 carboxyl groups. The capsule and a coumarin within it are illustrated in Figure 1. (See the chemical structure of OA in the Supporting Information (SI), Figure S1.) Three coumarin molecules, introduced in Figure 2, are investigated as guest molecules.

Electron transfer from the encapsulated coumarin to a freely dissolved electron acceptor in the aqueous solvent environment—across the molecular wall of a host cage—has been studied using femtosecond time-resolved optical spectroscopy with methyl viologen (MV^{2+}) as the water-soluble electron acceptor.[8,9] Nevertheless, there remains a need to account for the optoelectronic properties of the guest molecules. To achieve this goal, we develop computational models to explain at the molecular level measured spectral trends of the encapsulated coumarins.

We show that a primary effect of the capsule on the guest molecule is to partially screen the electrostatic environment due to the aqueous solution, and that this effect can be represented, when studying the spectra of the guest molecule, using an effective dielectric constant. In earlier studies by combining molecular dynamics (MD) simulations with NMR studies, we showed that molecules of the size of the considered coumarins

Received: June 6, 2017
Revised: June 20, 2017
Published: June 22, 2017

DOI: 10.1021/acs.jpcc.7b05522
J. Phys. Chem. C 2017, 121, 15481−15488

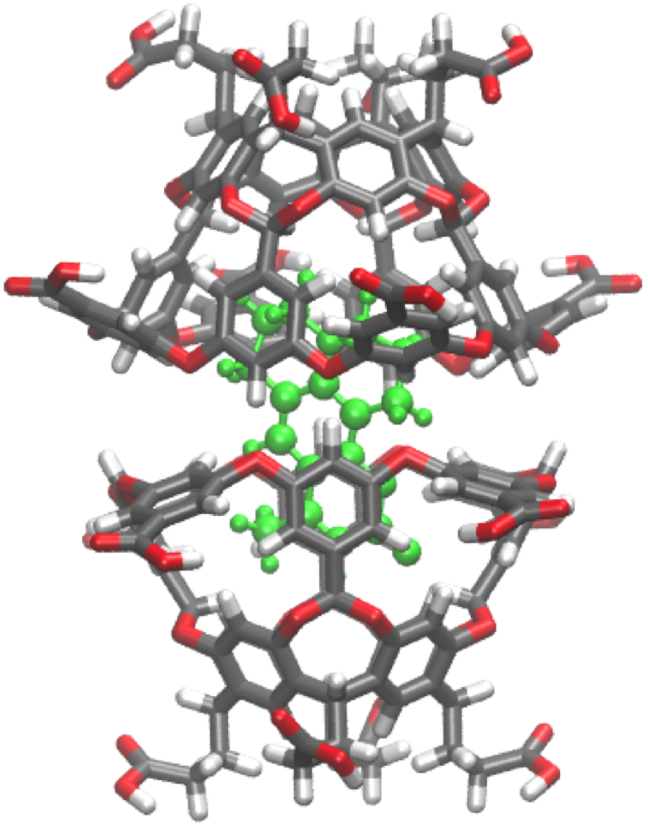

Figure 1. Octa-acid capsule with a C480 coumarin guest molecule. Coordinates of the optimized geometry at the B3LYP/6-31G(d) level are provided in the SI.

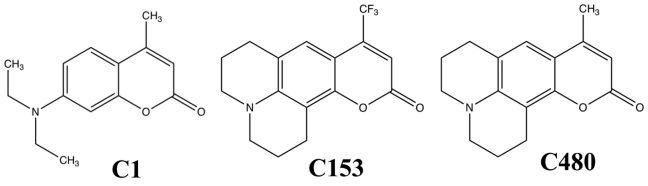

Figure 2. Considered coumarins: C1, C153, and C480. Coordinates of the optimized geometries at the B3LYP/6-31G(d) level are provided in the SI.

are expected to fit well, with no substantial distortion, within the capsule cavity.[13] We then address the fluorescence spectra, which are significantly blue-shifted upon encapsulation. In particular, we explain the capsule role to shield the dielectric environment, an effect that can be represented by an effective dielectric constant, which mitigates photoinduced charge transfer. Our computational studies associate the blue shift of the spectra (relative to those of the free solvated coumarins) to a partial CT process, where the capsule is the acceptor.

We employ time-dependent density functional theory (TDDFT)[14,15] with a polarizable continuum model (PCM)[16−20] to calculate coumarin spectra in various environments. Our computational approach has been used to study several CT processes providing unique insight at the molecular level, while reliably reproducing measured spectra.[21−24]

Our goal in this study is twofold: First, we provide an important benchmark of the calculated TDDFT/PCM excitation energies to reproduce measured absorption and fluorescence spectra of freely solvated dye molecules.[25] We then extend the approach to address the encapsulation effect on the coumarin spectra.

METHODS

Excited-state energies of solvated systems are calculated at two TDDFT/PCM levels. At the perturbative linear response (ptLR) level,[17] only the first order response to the reaction field representing the dielectric environment is invoked,[26,27] whereas at the perturbative state-specific (ptSS) level the effect of the dielectric on a specific excited state density is evaluated.[17,18,28−34] In either case, the solvent's optical dielectric constant is used to describe electronic polarization upon excitation.[17,18] Excited-state geometries used to calculate emission energies are optimized at the ptLR level.

We employ the range-separated hybrid (RSH) functional LRC-ωPBE,[35,36] which achieves reliable CT excitation energies in TDDFT calculations.[36−38] The success of RSH functionals in describing CT states builds on the proper description of the long-range exchange−correlation potential that leads to physically meaningful frontier orbitals.[39−42] The range-separation parameter is tuned for each dielectric constant following the J2 scheme.[43−46] All calculations were performed using Q-Chem v. 4.3.1.[47]

RESULTS AND DISCUSSION

Freely Solvated Coumarins. We start by analyzing the excited states of free coumarins in various solvents. The solvent dielectric constant strongly affects the frontier orbital energies, where the highest-occupied molecular orbitals (HOMOs) localize toward the amine group and the lowest-unoccupied MOs (LUMOs) are localized toward the carboxyl group. The frontier orbitals are illustrated in Figure 3 for two different dielectric constants: ε = 78.5, representing water, and ε = 3, representing a nonpolar solvent. For all three coumarin guests, the orbital gap decreases from over 7 eV in the gas phase to about 3 eV in aqueous solution. Similar destabilization of the HOMO is observed for all three coumarins; a relatively smaller stabilization is found for the LUMOs. However, for the C153 molecule that has a stronger electron withdrawing group (CF_3 substitution), the LUMO is stabilized by about 0.5 eV more than in the other two cases. The frontier orbital energies, ionization potentials (IPs), and electron affinities (EAs) calculated for several different solvent dielectric constants are listed in Table 1. (The dielectric constants are given in SI, Table S1.)

The RSH-based orbital energies are in good agreement with the IP/EA energies, whereas B3LYP values are underestimated, as expected from functionals that bear a constant fraction of exact exchange.[48−50] (B3LYP energies are listed in the SI, Table S2, with orbitals illustrated in Figure S2.) The range separation parameter (ω) is also quite strongly dependent on the solvent dielectrics, decreasing with the dielectric constant, indicating that the length scale at which long-range exchange is switched on increases with the dielectric constant. For all three coumarins, the tuned ω value drops by an order of magnitude moving from the gas phase into aqueous solution. For example, in C480 the ω parameter is 0.245 in the gas phase and 0.024 in water. Similar trends of decreasing range separation parameter due to the dielectric constant were reported in previous studies.[42,51,52]

We next benchmark the computational approach to calculate electronic excited states by considering the spectra of

DOI: 10.1021/acs.jpcc.7b05522
J. Phys. Chem. C 2017, 121, 15481−15488

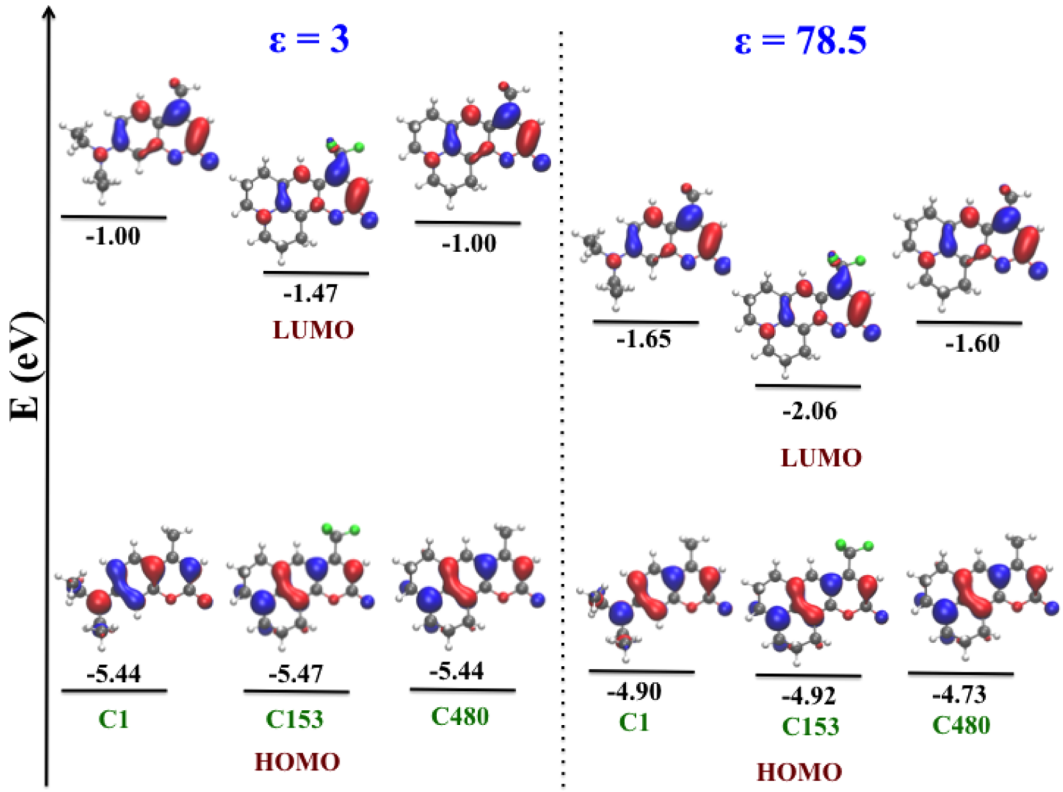

Figure 3. Frontier molecular orbital (MO) energies of C1, C153, and C480. The MOs are calculated at the LRC-ωPBE functional.

Table 1. HOMO and LUMO Energies, Ionization Potential (IP), and Electron Affinity (EA) Calculated at the Level of LRC-ωPBE/6-31G(d) in Different Solvents[a]

solvent	ω[b]	ε_H	ε_L	IP	EA
		C1			
gas	0.245	−7.10	0.43	−7.53	0.38
cyclohexane	0.100	−5.88	−0.57	−5.90	−0.53
ethyl acetate	0.045	−5.19	−1.28	−5.25	−1.20
ethanol	0.028	−4.95	−1.58	−5.04	−1.47
acetonitrile	0.026	−4.92	−1.60	−5.01	−1.50
glycerol	0.026	−4.92	−1.60	−5.50	−1.51
water	0.020	−4.90	−1.65	−4.99	−1.53
		C153			
gas	0.236	−7.13	0.13	−7.03	0.16
cyclohexane	0.097	−5.93	−1.03	−5.94	−0.98
ethyl acetate	0.045	−5.22	−1.71	−5.21	−1.61
ethanol	0.027	−4.98	−2.01	−5.04	−1.88
acetonitrile	0.026	−4.95	−0.07	−5.02	−1.91
glycerol	0.026	−4.92	−2.06	−5.01	−1.91
water	0.026	−4.92	−2.06	−4.99	−1.94
		C480			
gas	0.235	−6.88	0.44	−6.80	0.40
cyclohexane	0.090	−5.68	−0.54	−5.71	−0.50
ethyl acetate	0.045	−5.00	−1.22	−5.08	−1.16
ethanol	0.028	−4.79	−1.52	−4.87	−1.43
acetonitrile	0.028	−4.76	−1.55	−4.41	−1.31
glycerol	0.024	−4.76	−1.55	−4.39	−1.30
water	0.024	−4.73	−1.60	−4.81	−1.50

[a]Energies are in eV. [b]The range separation parameter, ω (in bohr^{-1}), that is tuned for each solvent.

coumarins in several solvents of dielectric constants ranging up to that of water.[25] Calculated excitation energies lie within 0.1 eV of measured values for all solvents except for ethyl acetate, where the errors are just a bit larger; see Table 2. Excitation energies computed with the cc-pVTZ basis set (see Table S3 in the SI) confirm that these values are converged with respect to basis set. (For the cc-pVTZ calculations, we use the ω parameter determined for 6-31G(d).) Calculated energies of higher excited states at various dielectric constant values are included in the SI, Figure S5.

All the low-lying $\pi-\pi^*$ S_1 states correspond to a HOMO−LUMO transition and therefore involve partial intramolecular CT, though still associated with a relatively large oscillator strength. Higher-energy states have oscillator strengths that are smaller by at least 1 order of magnitude. The red shift of the lowest excited-state energies increases with the polarity of the medium, reflecting the intramolecular CT character from the aromatic amine group (donor) to the carbonyl group (acceptor). The corresponding detachment−attachment densities of these CT states are illustrated in the SI, Figure S6, where these densities are as expected dominated by the HOMO and LUMO, respectively. The increase in the charge separation with the dielectric constant, $\Delta Q = |Q_{donor} - |Q_{acceptor}$, is quantified following the CHELPG population analysis.[53] (See values listed in Table 2.) The CHELPG population analysis scheme is known to achieve robust atomic charges showing only weak dependence on the basis set choice.[54] For completeness we list the corresponding charge transfer values based on the Mulliken population analysis that agree with the trend observed with the CHELPG values. (See comparison in SI, Table S4.)

The ptSS excitation energies are reproduced within 0.1 eV by the ptLR values (compare with SI, Table S5). We associate this trend with the relatively small transition dipole, as the donor/acceptor separation is <5 Å. Indeed, C153 exhibits the largest

DOI: 10.1021/acs.jpcc.7b05522
J. Phys. Chem. C 2017, 121, 15481−15488

Table 2. Calculated Absorption Energy (E_{abs}), Emission Energy (E_{em}), Stokes Shift (Δ), and Amount of Charge Transfer (ΔQ) for the Coumarins in Various Solvents[a]

solvent	E_{abs}	E_{em}	Δ	ΔQ
		C1		
cyclohexane	3.55 (3.54)	3.11 (3.14)	0.44 (0.40)	0.55
ethyl acetate	3.34 (3.43)	2.80 (2.98)	0.54 (0.45)	0.69
ethanol	3.28 (3.32)	2.67 (2.75)	0.61 (0.57)	0.73
acetonitrile	3.27 (3.38)	2.75 (2.88)	0.52 (0.50)	0.73
glycerol	3.26 (3.23)	2.77 (2.68)	0.49 (0.55)	0.74
water	3.26 (3.26)	2.73 (2.72)	0.53 (0.54)	0.74
		C153		
cyclohexane	3.16(3.16)	2.64 (2.73)	0.52 (0.43)	0.76
ethyl acetate	2.92 (3.03)	2.29 (2.48)	0.63 (0.55)	0.85
ethanol	2.88 (2.95)	2.28 (2.34)	0.60 (0.61)	0.86
acetonitrile	2.88 (2.97)	2.28 (2.38)	0.60 (0.59)	0.88
glycerol	2.88 (2.86)	2.28 (2.27)	0.60 (0.59)	0.88
water	2.86 (2.88)	2.26 (2.26)	0.60 (0.62)	0.87
		C480		
cyclohexane	3.43 (3.43)	2.92 (3.05)	0.51 (0.38)	0.67
ethyl acetate	3.19 (n/a)	2.64 (n/a)	0.55 (n/a)	0.80
ethanol	3.15 (3.20)	2.60 (2.62)	0.55 (0.58)	0.81
acetonitrile	3.14 (3.26)	2.59 (2.76)	0.55 (0.50)	0.83
glycerol	3.14 (n/a)	2.59 (n/a)	0.55 (n/a)	0.83
water	3.14 (3.13)	2.58 (2.54)	0.56 (0.59)	0.84

[a]The excited states are calculated using the state-specific TDDFT-PCM approach at the LRC-ωPBE/6-31G(d) level. Measured values[25] are provided in parentheses. (A graphic comparison is provided in Figure 4, where additional comparisons of the calculated absorption and emission energies are provided in SI Figures S3 and S4, respectively). Energies are listed in eV.

ΔQ and difference between the ptLR and ptSS values. As expected, the B3LYP excitation energies are substantially lower, by up to 0.7 eV as compared to LRC-ωPBE values in the gas phase. (For B3LYP values, see Table S6 in the SI.) Interestingly, the B3LYP PCM energies become larger than the LRC-ωPBE values upon increase of the dielectric constant (by 0.3 eV in water), reflecting a much weaker solvent dependence for B3LYP absorption energies. A similar trend has been reported previously.[55]

Encapsulated Coumarins. Next, we consider the spectra of the coumarins upon their encapsulation. We focus first on the absorption spectra, which are only moderately blue-shifted (by less than 0.2 eV) in comparison with those of coumarins in water. The measured values for the encapsulated and free coumarins in water are indicated by triangles in Figure 4. (These values are also listed in Table 3.)

We hypothesize that the role of the capsule environment can be represented as partially, though not completely, screening the solvent dielectric. We therefore calculate the absorption energies of the three coumarins in a range of dielectric constants up to that of water, which is the solvent of the encapsulated systems. In all of these calculations we use the same optical dielectric constant as that of water (ε_{opt} = 1.78). Optical dielectric constants vary only slightly for the different solvents considered in this work, where the ε_{opt} values range from 1.5 to 3.0.[57] (A refractive index n = 1.5 is typical for proteins,[58] corresponding to $\varepsilon_{opt} = n^2$ = 2.25.) The resulting absorption energies within a range of dielectric constants are listed in Table 3 and are also shown in Figure 4.

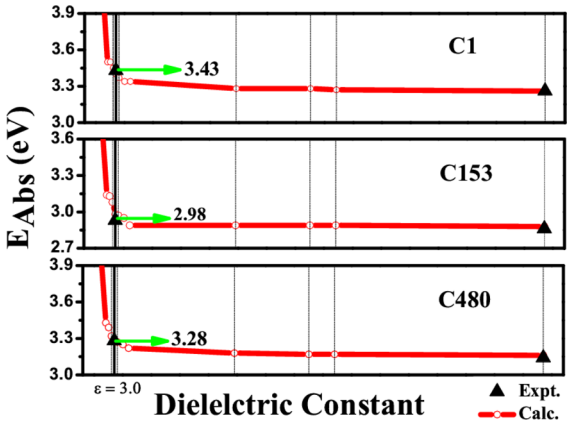

Figure 4. Calculated absorption energies of the coumarin molecules at various static dielectric constant values with the optical dielectric constant set to that of water (red line with circles), and measured absorption energies of coumarin@OA_2 in water (black triangles). (The values are listed in Table 3.)

Importantly, the encapsulated coumarin excitation energies are best reproduced using a dielectric constant of 3.0, with a root-mean-square deviation (RMSD) from the measured values of only 0.01 eV, compared to the much larger RMSD of 0.7 eV for gas phase calculated values. (RMSDs for various dielectric constants are listed in the SI, Table S7.) We relate this effective low dielectric constant of 3.0 to the typical constants of proteins, given that the OA_2 walls are made of carboxylic acid groups and benzene rings.

We further analyze the capsule's environmental effect by considering the excited state of C480 within an explicit capsule and within PCM. We find significant intermolecular CT from C480 to OA_2 for the excited state. In other words, the capsule acts as a charge acceptor limiting the intramolecular charge transfer in the excited state. This intermolecular CT character of the excited states of C480 in OA_2 is calculated using the LRC-ωPBE/6-31G(d) level making the Tamm−Dancoff approximation and with PCM (ε = 78.5) at a geometry optimized at the B3LYP/6-31G(d) level. As illustrated in Figure 5, the un-ionized form of the capsule was used as the host in this calculation. A large CT contribution is reflected by the CIS expansion coefficient of 0.47 for replacing the HOMO that is coumarin-localized with the LUMO + 8 orbital that is capsule-localized. (The HOMO−LUMO replacement, where both orbitals are localized on the coumarin molecule, has an expansion coefficient of 0.31.) This is consistent with population analysis of the excited state which finds 0.39e charge transfer based on CHELPG scheme (the Mulliken value is 0.35e).

Consequently, the C480 excited state molecular dipole moment (or ΔQ) is reduced in comparison to that in aqueous solution (no capsule). As discussed above for the solvated free coumarins, we find a relationship between the solvent dielectric and the amount of intramolecular CT. The free coumarin study exhibits that the extent of orbital polarization in the ground state affects the amount of charge transfer in the excited state. The encapsulation not only weakens the orbital polarization by screening the dielectric environment but also takes part in intermolecular charge transfer.

While we achieve a good agreement with the measured emission values for free coumarins in various solvents (Table 2), this is not the case for the encapsulated coumarins, for

DOI: 10.1021/acs.jpcc.7b05522
J. Phys. Chem. C 2017, 121, 15481−15488

Table 3. Dielectric Constant Dependence of the Calculated Absorption Energy (E_{abs}), Emission Energy (E_{em}), Stokes Shift (Δ), and Amount of Charge Transfer Computed at the LRC-ωPBE/6-31G(d) Level with the ptSS PCM Approach Based on the CHELPG Population Analysis of the Relevant State[a]

ε	E_{abs}	E_{em}	Δ	ΔQ
		C1		
1.0	4.24	3.85	0.39	0.08
2.5	3.50	3.04	0.46	0.60
3.0	3.45	2.96	0.49	0.64
3.0	**3.45**	**3.08***	**0.37**	
3.5	3.40	2.90	0.50	0.66
4.0	3.37	2.86	0.51	0.68
5.0	3.34	2.82	0.52	0.69
	–			
78.5	3.26	2.73	0.53	0.74
	3.43[b]	3.02[b]	0.41[b]	
		C153		
1.0	3.91	3.60	0.31	0.34
2.5	3.03	2.48	0.55	0.79
3.0	2.99	2.33	0.66	0.82
3.0	**2.99**	**2.63***	**0.36**	
3.5	2.95	2.31	0.64	0.83
4.0	2.94	2.30	0.64	0.84
5.0	2.93	2.29	0.64	0.85
	–			
78.5	2.86	2.26	0.60	0.87
	2.93[b]	2.57[b]	0.36[b]	
		C480		
1.0	4.10	3.85	0.25	0.46
2.5	3.35	2.80	0.55	0.71
3.0	3.29	2.75	0.54	0.75
3.0	**3.29**	**2.95***	**0.34**	
3.5	3.25	2.71	0.54	0.77
4.0	3.23	2.69	0.54	0.78
5.0	3.22	2.67	0.55	0.78
	–			
78.5	3.14	2.58	0.56	0.84
	3.28[b]	2.92[b]	0.36[b]	

[a]The optical dielectric constant of water is used. The RMSD from the measured absorption values (see SI, Table S7) is minimized with ε = 3.0. Emission energies calculated at CDFT-optimized geometries of a reduced charge transfer are indicated by (*). The measured values[S6] are also listed. (A comparison of the charge transferred using the CHELPG population analysis to Mulliken based charges is provided in the SI, Table S4.) [b]Measured at capsule.

which the calculated energies overestimate the Stokes shift. The emission energies of the encapsulated molecules are calculated with the same effective dielectric constant as used for the absorption energies (see Table 3). This overestimation of the Stokes shift increases with the amount of the intramolecular CT, which is 0.6*e*, 0.7*e*, and 0.8*e* for C1, C480, and C153, respectively.

To better address the emission shift of the encapsulated coumarins using PCM-TDDFT calculations, we need to understand the limitations of the model. In the absorption study, we adjust the solvent dielectric to engender the reduction of the intramolecular CT due to the locally excited state of the coumarin mixing with the intermolecular charge-transfer state of the encapsulated system. However, we do not include the information on the intermolecular CT state, which

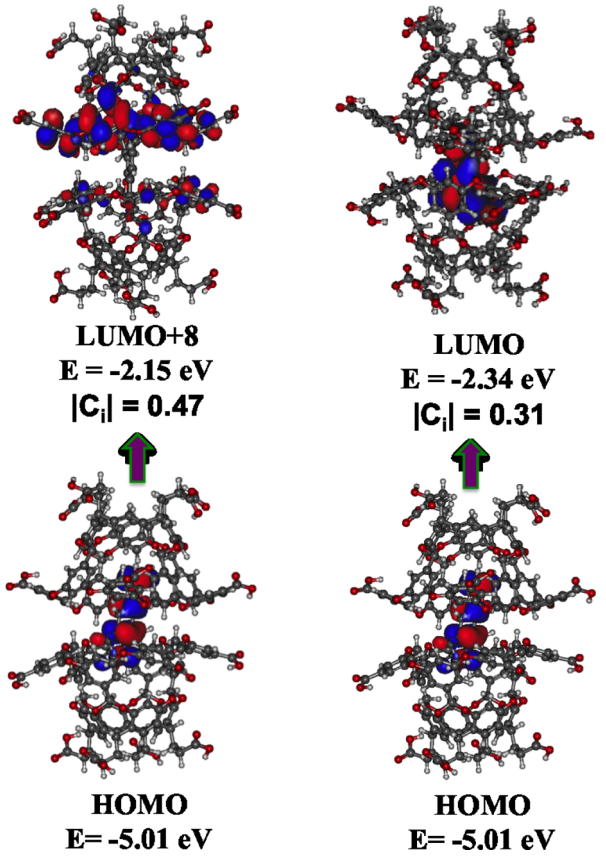

Figure 5. Key molecular orbitals (MOs) involved in excited state of C480@OA_2 calculated with TDDFT using LRC-wPBE functional. The expansion coefficient representing CT to the capsule bears the largest value in the calculated expansion with 0.47.

is required while performing excited-state geometry optimization, and thus the structural relaxation is overestimated. In other words, the capsule-related intermolecular charge transfer upon excitation reduces the structural relaxation and therefore blue-shifts the emission energy compared to that of the free solvated molecule.

To understand the relationship between CT and structural relaxation, we follow the ester group bond lengths in C480 upon adjusting the amount of charge that is transferred within the coumarin using charge constrained density functional theory[S9,60] (CDFT) optimizations (see SI, Figure S7). We then relate the CDFT geometries obtained with 0.0*e* and with 0.7*e* transferred within the molecule to the ground state (absorption) and excited state (emission) geometries, respectively. This important assignment of CDFT geometries is supported by following key bond lengths (see bond lengths provided in SI, Figure S7, and listed in SI, Table S8) and excitation energies (see SI, Table S9).

Next, we consider CDFT-optimized geometries in which the intramolecular CT is set to a lower 0.35*e* (compared to the free coumarin range of CT of 0.6–0.8*e*). These results are indicated by asterisks (*) in Table 3 and represent the emissive encapsulated state. (The capsule was indicated above to function as an acceptor of 0.35*e* in an intermolecular process when calculated with C480.) Indeed, the excitation energies calculated at these (*) geometries are in excellent agreement (within 0.1 eV) with the measured emission energies of the encapsulated coumarins. We therefore support the hypothesis

DOI: 10.1021/acs.jpcc.7b05522
J. Phys. Chem. C 2017, 121, 15481–15488

that the capsule acts as a charge acceptor that reduces the coumarin-based intramolecular CT of the emissive state, therefore mitigating its structural relaxation.

CONCLUSIONS

The molecular environment of dye molecules hosted in octa-acid capsules solvated in water is investigated by computational models and compared against available absorption and emission spectra. We hypothesize that the capsule screens only partially the solvent dielectric. As a result, the absorption spectrum is shown to be reproduced well by state-of-the-art calculations based on a polarizable continuum model used in TDDFT. Excitation energies obtained with an effective dielectric constant of 3.0 reproduce the measured absorption spectra of the encapsulated coumarins quite well. We then analyze the emission spectra. Here, we hypothesize that the observed reduced Stokes shift upon encapsulation is due to the capsule's role in limiting the relaxation of the excited state as it accepts charge and therefore decreases the intramolecular charge transfer within the coumarin. Our calculated emission energies with constrained ester bonds or upon reduced CT present a substantially improved agreement with the measured values compared with the energies calculated with unconstrained geometries.

ASSOCIATED CONTENT

Supporting Information

The Supporting Information is available free of charge on the ACS Publications website at DOI: 10.1021/acs.jpcc.7b05522.

Frontier molecular orbitals of the coumarins calculated using B3LYP, graphical representation of the capsule, graphical representation of calculated and measured absorption and emission energies in several solvents, solvent dielectric constants, HOMO/LUMO and IP/EA at different solvents using B3LYP functional, absorption and emission energies at different solvents compared to experimental values using CC-pVTZ, ptLR, B3LYP, energies of several excited states, detachment-attachment density plots, Mulliken, and CHELPG based population analysis, RMSDs of calculated absorption energies from measured values of capsulated systems at different dielectric constants, analysis of bond length upon varying the intramolecular charge transfer in C480, and *XYZ* coordinates of the coumarins (PDF)

AUTHOR INFORMATION

Corresponding Authors

*E-mail: murthy1@miami.edu.
*E-mail: cxb77@case.edu.
*E-mail: herbert@chemistry.ohio-state.edu.
*E-mail: bdunietz@kent.edu. Tel.: 330-672-2032. Fax: 330-672-3816.

ORCID

Zilong Zheng: 0000-0003-4310-2755
Vaidhyanathan Ramamurthy: 0000-0002-3168-2185
Clemens Burda: 0000-0002-7342-2840
John M. Herbert: 0000-0002-1663-2278
Barry D. Dunietz: 0000-0002-6982-8995

Present Address

⊥Z.-Q.Y.: Q-Chem, Inc., 6601 Owens Drive, Suite 105, Pleasanton, CA 94588, USA.

Notes

The authors declare no competing financial interest.

ACKNOWLEDGMENTS

B.D.D. acknowledges National Science Foundation (NSF) Grant CHE-1362504. We are also grateful to generous resource allocations on the Ohio Supercomputer Center[61] and the Kent State University, College of Arts and Sciences Computing Cluster. V.R. thanks the NSF (CHE-1411458) for financial support. Work by Z.-Q.Y. and J.M.H. was supported by National Science Foundation Grant CHE-1300603, by a Camille Dreyfus Teacher–Scholar Award (to J.M.H.), and by a fellowship from the Alexander von Humboldt Foundation (to J.M.H.).

REFERENCES

(1) Li, Y. Molecular design of photovoltaic materials for polymer solar cells: toward suitable electronic energy levels and broad absorption. *Acc. Chem. Res.* **2012**, *45*, 723–733.
(2) Oevering, H.; Verhoeven, J.; Paddon-Row, M.; Warman, J. Charge-transfer absorption and emission resulting from long-range through-bond interaction; exploring the relation between electronic coupling andelectron-transfer in bridged donor-acceptor systems. *Tetrahedron* **1989**, *45*, 4751–4766.
(3) Liddell, P. A.; Kuciauskas, D.; Sumida, J. P.; Nash, B.; Nguyen, D.; Moore, A. L.; Moore, T. A.; Gust, D. Photoinduced Charge Separation and Charge Recombination to a Triplet State in Carotene-Porphyrin-Fullerene Triad. *J. Am. Chem. Soc.* **1997**, *119*, 1400–1405.
(4) Davis, W. B.; Svec, W. A.; Ratner, M. A.; Wasielewski, M. R. Molecular-wire behaviour in p-phenylenevinylene oligomers. *Nature* **1998**, *396*, 60–63.
(5) Ricks, A. B.; Solomon, G. C.; Colvin, M. T.; Scott, A. M.; Chen, K.; Ratner, M. A.; Wasielewski, M. R. Controlling Electron Transfer in Donor- Bridge- Acceptor Molecules Using Cross-Conjugated Bridges. *J. Am. Chem. Soc.* **2010**, *132*, 15427–15434.
(6) Closs, G.; Calcaterra, L.; Green, N.; Penfield, K.; Miller, J. Distance, stereoelectronic effects, and the Marcus inverted region in intramolecular electron transfer in organic radical anions. *J. Phys. Chem.* **1986**, *90*, 3673–3683.
(7) Oevering, H.; Paddon-Row, M. N.; Heppener, M.; Oliver, A. M.; Cotsaris, E.; Verhoeven, J. W.; Hush, N. S. Long-range photoinduced through-bond electron transfer and radiative recombination via rigid nonconjugated bridges: distance and solvent dependence. *J. Am. Chem. Soc.* **1987**, *109*, 3258–3269.
(8) Porel, M.; Klimczak, A.; Freitag, M.; Galoppini, E.; Ramamurthy, V. Photoinduced electron transfer across a molecular wall: coumarin dyes as donors and methyl viologen and TiO_2 as acceptors. *Langmuir* **2012**, *28*, 3355–3359.
(9) Porel, M.; Chuang, C.-H.; Burda, C.; Ramamurthy, V. Ultrafast photoinduced electron transfer between an incarcerated donor and a free acceptor in aqueous solution. *J. Am. Chem. Soc.* **2012**, *134*, 14718–14721.
(10) Yu, G.; Jie, K.; Huang, F. Supramolecular amphiphiles based on host-guest molecular recognition motifs. *Chem. Rev.* **2015**, *115*, 7240–7303.
(11) Son, H.-J.; Wang, X.; Prasittichai, C.; Jeong, N. C.; Aaltonen, T.; Gordon, R. G.; Hupp, J. T. Glass-encapsulated light harvesters: more efficient dye-sensitized solar cells by deposition of self-aligned, conformal, and self-limited silica layers. *J. Am. Chem. Soc.* **2012**, *134*, 9537–9540.
(12) Porel, M.; Jayaraj, N.; Kaanumalle, L. S.; Maddipatla, M. V.; Parthasarathy, A.; Ramamurthy, V. Cavitand octa acid forms a nonpolar capsuleplex dependent on the molecular size and hydrophobicity of the guest. *Langmuir* **2009**, *25*, 3473–3481.
(13) Choudhury, R.; Barman, A.; Prabhakar, R.; Ramamurthy, V. Hydrocarbons depending on the chain length and head group adopt

different conformations within a water-soluble nanocapsule: 1H NMR and molecular dynamics studies. *J. Phys. Chem. B* **2013**, *117*, 398−407.
(14) Casida, M. E. Time-dependent density-functional theory for molecules and molecular solids. *J. Mol. Struct.: THEOCHEM* **2009**, *914*, 3−18.
(15) Liu, J.; Liang, W. Z. Analytical Hessian of electronic excited states in time-dependent density functional theory with Tamm-Dancoff approximation. *J. Chem. Phys.* **2011**, *135*, 014113.
(16) Lange, A. W.; Herbert, J. M. A smooth, nonsingular, and faithful discretization scheme for polarizable continuum models: The switching/Gaussian approach. *J. Chem. Phys.* **2010**, *133*, 244111.
(17) Mewes, J.-M.; You, Z.-Q.; Wormit, M.; Kriesche, T.; Herbert, J. M.; Dreuw, A. Experimental benchmark data and systematic evaluation of two a posteriori, polarizable-continuum corrections for vertical excitation energies in solution. *J. Phys. Chem. A* **2015**, *119*, 5446−5464.
(18) You, Z.-Q.; Mewes, J.-M.; Dreuw, A.; Herbert, J. M. Comparison of the Marcus and Pekar partitions in the context of non-equilibrium, polarizable-continuum solvation models. *J. Chem. Phys.* **2015**, *143*, 204104.
(19) Mennucci, B.; Scalmani, G.; Jacquemin, D. Excited-state vibrations of solvated molecules: Going beyond the linear-response polarizable continuum model. *J. Chem. Theory Comput.* **2015**, *11*, 847−850.
(20) Herbert, J. M.; Lange, A. W. In *Many-Body Effects and Electrostatics in Biomolecules*; Cui, Q., Ren, P., Meuwly, M., Eds.; Pan Stanford: 2016; Chapter 11, pp 363−416.
(21) Zheng, S.; Phillips, H.; Geva, E.; Dunietz, B. D. *Ab-initio* Study of the Emissive Charge-Transfer States of Solvated Chromophore-Functionalized Silsesquioxanes. *J. Am. Chem. Soc.* **2012**, *134*, 6944−6947.
(22) Lee, M. H.; Dunietz, B. D.; Geva, E. Calculation from First Principles Intramolecular Golden-rule rate constants for Photoinduced Electron Transfer in Molecular Donor-Acceptor Systems. *J. Phys. Chem. C* **2013**, *117*, 23391−23401.
(23) Zheng, Z.; Manna, A. K.; Hendrickson, H. P.; Hammer, M.; Song, C.; Geva, E.; Dunietz, B. D. Molecular Structure, Spectroscopy, and Photoinduced Kinetics in Trinuclear Cyanide Bridged Complex in Solution: A First-Principles Perspective. *J. Am. Chem. Soc.* **2014**, *136*, 16954−16957.
(24) Manna, A. K.; Balamurugan, D.; Cheung, M. S.; Dunietz, B. D. Unraveling the Mechanism of Photoinduced Charge Transfer in Carotenoid-Porphyrin-C60 Molecular Triad. *J. Phys. Chem. Lett.* **2015**, *6*, 1231−1237.
(25) Jones, G., II; Jackson, W. R.; Choi, Y. C.; Bergmark, W. R. Solvent Effects on Emission Yield and Lifetime for Coumarin Laser Dyes. Requirements for a Rotatory Decay Mechanism. *J. Phys. Chem.* **1985**, *89*, 294−300.
(26) Cammi, R.; Mennucci, B. Linear response theory for the polarizable continuum model. *J. Chem. Phys.* **1999**, *110*, 9877−9886.
(27) Cossi, M.; Barone, V. Time-dependent density functional theory for molecules in liquid solutions. *J. Chem. Phys.* **2001**, *115*, 4708−4717.
(28) Tomasi, J.; Persico, M. Molecular interactions in solution: an overview of methods based on continuous distributions of the solvent. *Chem. Rev.* **1994**, *94*, 2027−2094.
(29) Cammi, R.; Tomasi, J. Nonequilibrium solvation theory for the polarizable continuum model: A new formulation at the SCF level with application to the case of the frequency-dependent linear electric response function. *Int. J. Quantum Chem.* **1995**, *56*, 465−474.
(30) Cossi, M.; Barone, V. Separation between fast and slow polarizations in continuum solvation models. *J. Phys. Chem. A* **2000**, *104*, 10614−10622.
(31) Improta, R.; Barone, V.; Scalmani, G.; Frisch, M. J. A state-specific polarizable continuum model time dependent density functional theory method for excited state calculations in solution. *J. Chem. Phys.* **2006**, *125*, 054103.
(32) Cammi, R. Coupled-cluster theories for the polarizable continuum model. II. Analytical gradients for excited states of molecular solutes by the equation of motion coupled-cluster method. *Int. J. Quantum Chem.* **2010**, *110*, 3040−3052.
(33) Cammi, R.; Fukuda, R.; Ehara, M.; Nakatsuji, H. Symmetry-adapted cluster and symmetry-adapted cluster-configuration interaction method in the polarizable continuum model: Theory of the solvent effect on the electronic excitation of molecules in solution. *J. Chem. Phys.* **2010**, *133*, 024104.
(34) Caricato, M. Absorption and Emission Spectra of Solvated Molecules with the EOM−CCSD−PCM Method. *J. Chem. Theory Comput.* **2012**, *8*, 4494−4502.
(35) Vydrov, O. A.; Scuseria, G. E. Assessment of a long-range corrected hybrid functional. *J. Chem. Phys.* **2006**, *125*, 234109−234117.
(36) Rohrdanz, M. A.; Martins, K. M.; Herbert, J. M. A long-range-corrected density functional that performs well for both ground-state properties and time-dependent density functional theory excitation energies, including charge-transfer excited states. *J. Chem. Phys.* **2009**, *130*, 054112.
(37) Laurent, A. D.; Jacquemin, D. TD-DFT benchmarks: A review. *Int. J. Quantum Chem.* **2013**, *113*, 2019−2039.
(38) Jacquemin, D.; Moore, B.; Planchat, A.; Adamo, C.; Autschbach, J. Performance of an optimally tuned range-separated hybrid functional for 0−0 electronic excitation energies. *J. Chem. Theory Comput.* **2014**, *10*, 1677−1685.
(39) Stein, T.; Autschbach, J.; Govind, N.; Kronik, L.; Baer, R. Curvature and Frontier Orbital Energies in Density Functional Theory. *J. Phys. Chem. Lett.* **2012**, *3*, 3740−3744.
(40) Kronik, L.; Stein, T.; Refaely-Abramson, S.; Baer, R. Excitation Gaps of Finite-Sized Systems from Optimally Tuned Range-Separated Hybrid Functionals. *J. Chem. Theory Comput.* **2012**, *8*, 1515−1531.
(41) Phillips, H.; Geva, E.; Dunietz, B. D. Calculating off-site excitations in symmetric donor-acceptor systems via time-dependent density functional theory with range-separated density functionals. *J. Chem. Theory Comput.* **2012**, *8*, 2661−2668.
(42) Phillips, H.; Zheng, Z.; Geva, E.; Dunietz, B. D. Orbital Gap Predictions for Rational Design of Organic Photovoltaic Materials. *Org. Electron.* **2014**, *15*, 1509−1520.
(43) Refaely-Abramson, S.; Sharifzadeh, S.; Jain, M.; Baer, R.; Neaton, J. B.; Kronik, L. Gap renormalization of molecular crystals from density-functional theory. *Phys. Rev. B: Condens. Matter Mater. Phys.* **2013**, *88*, 081204R.
(44) Kuritz, N.; Stein, T.; Baer, R.; Kronik, L. Charge-Transfer-Like $\pi - pi^*$ Excitations in Time-Dependent Density Functional Theory: A Conundrum and Its Solution. *J. Chem. Theory Comput.* **2011**, *7*, 2408−2415.
(45) Stein, T.; Kronik, L.; Baer, R. Prediction of charge-transfer excitations in coumarin-based dyes using a range-separated functional tuned from first principles. *J. Chem. Phys.* **2009**, *131*, 244119.
(46) Grimme, S.; Neese, F. Double-hybrid density functional theory for excited electronic states of molecules. *J. Chem. Phys.* **2007**, *127*, 154116.
(47) Shao, Y.; Gan, Z.; Epifanovsky, E.; Gilbert, A. T.; Wormit, M.; Kussmann, J.; Lange, A. W.; Behn, A.; Deng, J.; Feng, X.; et al. Advances in molecular quantum chemistry contained in the Q-Chem 4 program package. *Mol. Phys.* **2015**, *113*, 184−215.
(48) Lee, C.; Yang, W.; Parr, R. G. Development of the Colle-Salvetti correlation-energy formula into a functional of the electron density. *Phys. Rev. B: Condens. Matter Mater. Phys.* **1988**, *37*, 785.
(49) Becke, A. D. A new mixing of Hartree-Fock and local density-functional theories. *J. Chem. Phys.* **1993**, *98*, 1372−1377.
(50) Perdew, J. P.; Burke, K.; Ernzerhof, M. Generalized gradient approximation made simple. *Phys. Rev. Lett.* **1996**, *77*, 3865.
(51) de Queiroz, T. B.; Kümmel, S. Charge-transfer excitations in low-gap systems under the influence of solvation and conformational disorder: Exploring range-separation tuning. *J. Chem. Phys.* **2014**, *141*, 084303.
(52) Sun, H.; Ryno, S.; Zhong, C.; Ravva, M. K.; Sun, Z.; Körzdörfer, T.; Bredas, J.-L. Ionization Energies, Electron Affinities, and Polarization Energies of Organic Molecular Crystals: Quantitative Estimations from a Polarizable Continuum Model (PCM)−Tuned

DOI: 10.1021/acs.jpcc.7b05522
J. Phys. Chem. C 2017, 121, 15481−15488

Range-Separated Density Functional Approach. *J. Chem. Theory Comput.* **2016**, *12*, 2906−2916.
(53) Breneman, C. M.; Wiberg, K. B. Determining atom-centered monopoles from molecular electrostatic potentials. The need for high sampling density in formamide conformational analysis. *J. Comput. Chem.* **1990**, *11*, 361−373.
(54) Jacquemin, D.; Le Bahers, T.; Adamo, C.; Ciofini, I. What is the "best" atomic charge model to describe through-space charge-transfer excitations? *Phys. Chem. Chem. Phys.* **2012**, *14*, 5383−5388.
(55) Guido, C. A.; Mennucci, B.; Jacquemin, D.; Adamo, C. Planar vs. twisted intramolecular charge transfer mechanism in Nile Red: new hints from theory. *Phys. Chem. Chem. Phys.* **2010**, *12*, 8016−8023.
(56) Gupta, S.; Adhikari, A.; Mandal, A. K.; Bhattacharyya, K.; Ramamurthy, V. Ultrafast singlet-singlet energy transfer between an acceptor electrostatically attached to the walls of an organic capsule and the enclosed donor. *J. Phys. Chem. C* **2011**, *115*, 9593−9600.
(57) See http://www.stenutz.eu/chem/solv23.php for a list of indices of refraction for common solvents.
(58) Hand, D. B. The refractivity of protein solutions. *J. Biol. Chem.* **1935**, *108*, 703−707.
(59) Wu, Q.; Van Voorhis, T. Direct optimization method to study constrained systems within density-functional theory. *Phys. Rev. A: At., Mol., Opt. Phys.* **2005**, *72*, 024502.
(60) Wu, Q.; Van Voorhis, T. Extracting electron transfer coupling elements from constrained density functional theory. *J. Chem. Phys.* **2006**, *125*, 164105.
(61) Ohio Supercomputer Center. http://osc.edu/ark:/19495/f5s1ph73, 1987.

DOI: 10.1021/acs.jpcc.7b05522
J. Phys. Chem. C 2017, 121, 15481−15488